Supporting Information (SI)

Three-Dimensional Co(II)-Metal−Organic Frameworks with Varying Porosities and Open Metal Sites toward Multipurpose Heterogeneous Catalysis under Mild Conditions

Santanu Chand[I], Shyam Chand Pal[I], Manas Mondal, Subrata Hota, Arun Pal, Rupam Sahoo and Madhab C. Das*

Department of Chemistry, Indian Institute of Technology Kharagpur, Kharagpur 721302 West Bengal, India.

E-mail: mcdas@chem.iitkgp.ac.in

Physical Measurements

Elemental analyses (C, H, N) were performed on an Elementar, Vario Micro Cube elemental analyser. FT-IR spectra (KBr pellets) were recorded on a PerkinElmer RX1 spectrophotometer. Powder X-ray diffraction (PXRD) data were collected (Cu Kα radiation of 1.5418 Å) on a Bruker D8 Advance diffactometer. Thermogravimetric analysis (TGA) was executed with a TG 209 *F3* Tarsus (Netzsch), and the sample was heated from room temperature to 800 °C at 5 °C min^{-1} rate under N_2 gas flow. ^{1}H, ^{13}C NMR spectrum was recorded using a Bruker Avance II 400 spectrometer. Mass spectrum was obtained using a Bruker MALDITOF/TOF spectrometer. Gas sorption experiments were performed using a Micromeritics ASAP 2020 Surface Characterization Analyser at different temperatures. All the guest solvents in the framework were exchanged with dry chloroform at least 10 times within 3 d, and the framework was evacuated at 373 K for 14 h until an outgas rate of 5 μmHg min^{-1} was achieved. The sorption measurement was maintained at 195 K by using methanol/dry ice mixture. A chiller was used for adsorption isotherms at 273 and 295 K, respectively.

Single Crystal X-ray Diffraction

The crystal and refinement data for **1** and **2** were collected in Table S1. In this case, a crystal of appropriate size was selected from the mother liquor and immersed in paratone oil and then it was mounted on the tip of a glass fibre and cemented using epoxy resin. Single crystal X-ray data were collected at 100/298 K on a Bruker SMART APEX II CCD diffractometer using graphite-monochromated Mo-K_α radiation (0.71073 Å). The linear absorption coefficients, scattering factors for the atoms and the anomalous dispersion corrections were taken from International Tables for X-ray Crystallography. The data integration and reduction were processed with SAINT[1] software. An empirical absorption

correction was applied to the collected reflections with SADABS using XPREP.[2] The structure was solved by the direct method using SHELXTL[3] and was refined on F^2 by full-matrix least-squares technique using the SHELXL-2014[4] program package. For all the cases non-hydrogen atoms were refined anisotropically. Selected bond lengths and bond angles are listed in Table S2 and S4.

Table S1: Crystal data and structure refinements for **1** and **2**.

	1	**2**
Empirical formula	'C_{40} H_{42} N_6 O_{14} Co_2'	'C_{14} H_{14} Co N_4 O_6'
Formula weight	948.66	393.22
Temperature(K)	100(1)	298(1)
Radiation	Mo-Kα	Mo-Kα
Wavelength(λ)	0.71073Å	0.71073Å
Crystal system	Monoclinic	Monoclinic
Space group	$P2_1/n$	$C2/c$
a[Å]	14.975(3)	14.785(3)
b[Å]	16.724(3)	16.325(3)
c[Å]	18.632(4)	7.539(2)
α[°]	90	90
β[°]	112.57(3)	102.51(3)
γ[°]	90	90
Volume[Å^3]	4308.9(18)	1776.5(7)
Z	4	4
Density (calculated) [Mg/m^3]	1.462	1.470
F(000)	1960	804
Refl. used [$I > 2\sigma(I)$]	5846	1499
Independent reflections	8979	1813
R_{int}	0.0846	0.0266
Refinement method	full-matrix least squares on F^2	full-matrix least squares on F^2
GOF	1.096	1.177
Final R indices[I>2σ(I)]	R_1= 0.0564, wR_2= 0.1481	R_1= 0.0923, wR_2= 0.3116
R indices (all data)	R_1= 0.0946, wR_2= 0.1675	R_1= 0.1002, wR_2= 0.3238

Table S2: Selected Bond Distances (Å) and Bond Angles (°) in **1**

Co1 − O1	2.058(3)	Co1 − O3	2.029(3)	Co1 − O6	2.040(3)
Co1 − O8	2.063(3)	Co1 − N1	2.127(4)	Co1 − OW3	2.178(3)
Co2− O4	2.059(3)	Co2 − O5	2.112(3)	Co2 − N3	2.218(3)
Co2 − OW1	2.012(3)	Co2 − OW2	2.063(3)	Co2 − OW3	2.067(3)

O3 − Co1 − O6	92.74(15)	O3 − Co1 − O1	90.01(15)
O6 − Co1 − O1	174.55(12)	O3 − Co1 − O8	178.56(15)
O6 − Co1 − O8	88.69(15)	O1 − Co1 − O8	88.55(15)
O3 − Co1 − N1	90.49(13)	O6 − Co1 − N1	85.92(12)
O1 − Co1 − N1	89.35(12)	O8 − Co1 − N1	89.46(13)
O3 − Co1 − OW3	90.28(12)	O6 − Co1 − OW3	93.64(12)
O1 − Co1 − OW3	91.05(11)	O8 − Co1 − OW3	89.78(12)
N1 − Co1 − OW3	179.13(12)	O4 − Co2 − OW2	92.32(13)
O4 − Co2 − OW3	93.73(11)	OW2 − Co2 − OW3	173.85(13)
O4 − Co2 − OW1	175.05(12)	OW2 − Co2 − OW1	84.23(14)
OW3 − Co2 − OW	1 89.66(13)	O4 − Co2 − O5	94.73(11)
OW2 − Co2 − O5	87.48(12)	OW3 − Co2 − O5	93.09(11)
OW1 − Co2 − O5	88.69(11)	O4 − Co2 − N3	86.55(11)
OW2 − Co2 − N3	90.62(13)	OW3 − Co2 − N3	88.67(11)

Table S3: H-bonding interactions in **1**

D − H…A	d(H…A) (Å)	D(D…A) (Å)	< DHA (^{O})
OW1 − H1W1…OW4	2.155(3)	2.778(2)	158.57(12)
OW1 − H2W1…O5	1.801(2)	2.731(3)	154.65(10)
OW2 − H1W2…O13	1.754(3)	2.643(4)	171.64(12)
OW2 − H2W2…OW4	2.084(3)	2.779(4)	165.45(10)
OW3 − H1W3…O2	1.758(3)	2.557(3)	160.76(8)
OW3 − H2W3…O7	1.725(3)	2.595(2)	165.32(11)
OW4 − H1W4…O7	1.751(3)	2.646(2)	150.87(11)
OW4 − H2W4…O12	1.920(3)	2.738(3)	155.20(8)

Table S4: Selected Bond Distances (Å) and Bond Angles (^{o}) in **2**

Co1 − O1	2.067(3)	Co1 − N1	2.173(4)
Co1 − OW1	2.0758(7)		

O1 − Co1 − OW1	90.35(10)	O1 − Co1 − OW1	89.65(10)
OW1 − Co1 − OW1	180.0	O1 − Co1 − N1	89.77(17)
O1 − Co1 − N1	90.23(17)	OW1 − Co1 − N1	90.88(11)
OW1 − Co1 − N1	89.13(11)	N1 − Co1 − N1	180.0
C1 − O1 − Co1	124.7(5)	O1 − Co1 − O1	180.0

Table S5: Non-bonding or H-bonding interactions in **2**

D − H…A	d(H…A) (Å)	D(D…A) (Å)	< DHA (^{O})
C5 − H5 …OW1	2.536(3)	3.432(2)	161.94(12)
OW1 − H1W1…O2	1.899(2)	2.682(3)	155.33(10)

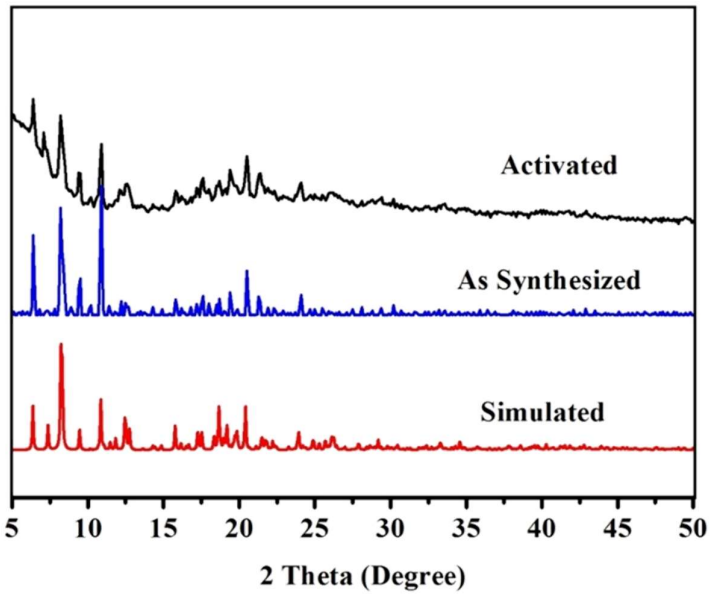

Figure S1: The PXRD pattern of simulated (red), as synthesized (blue) and after activation (black) of **1**.

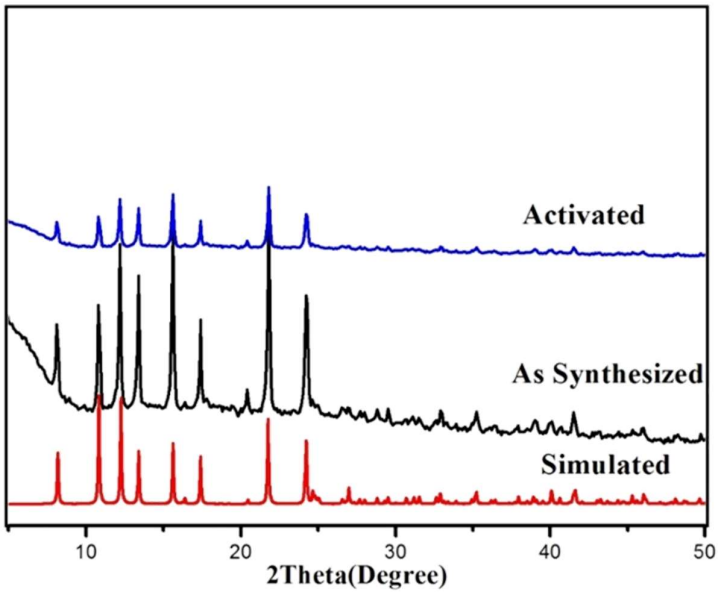

Figure S2: The PXRD pattern of simulated (red), as synthesized (black) and after activation (blue) of **2**.

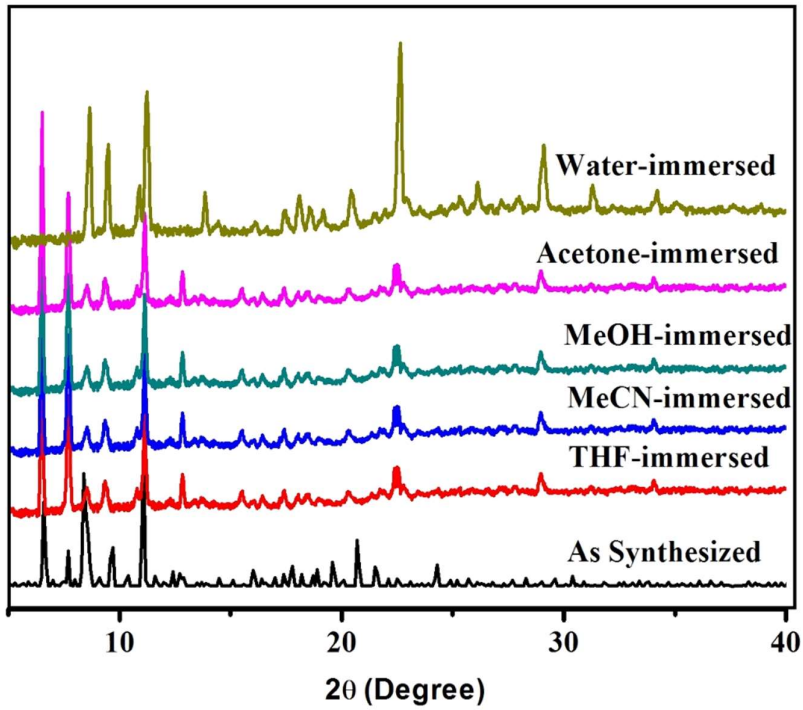

Figure S3: The PXRD pattern of **1** in different common organic solvent comparing with as synthesized one.

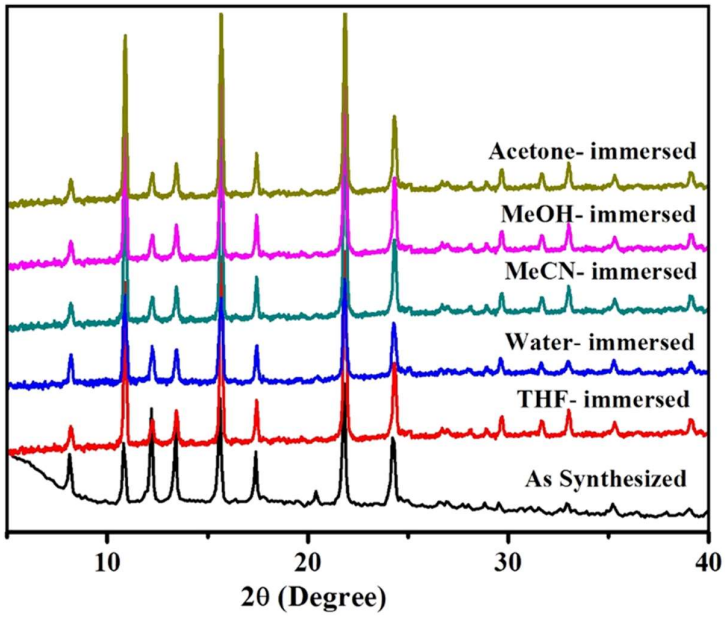

Figure S4: The PXRD pattern of **2** in different common organic solvent comparing with as synthesized one.

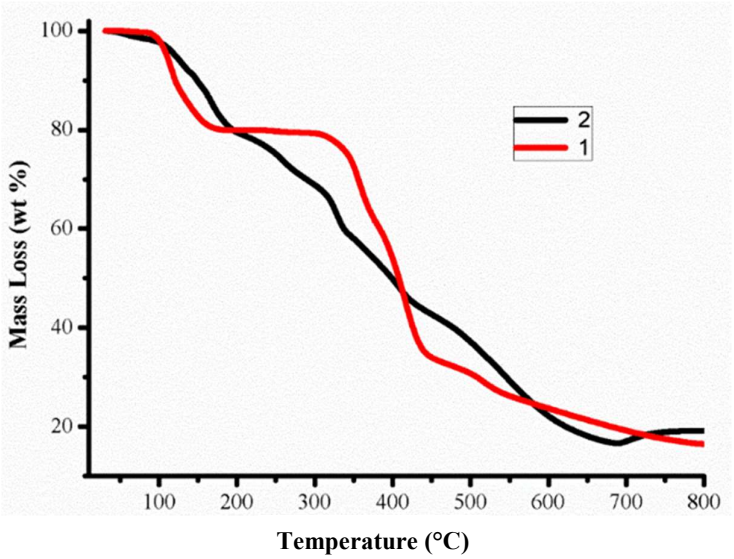

Figure S5: Thermo gravimetric analysis profile of **1** and **2**.

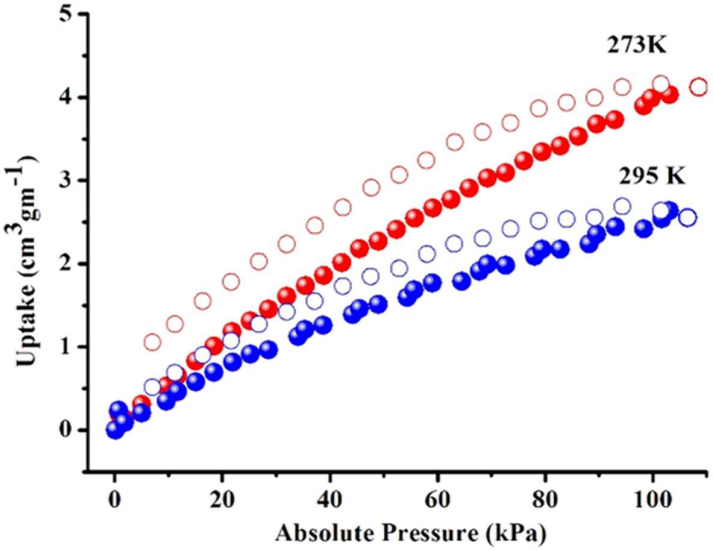

Figure S6: CO_2 sorption isotherms of **2a** at 273 and 295 K (Solid and open symbols represent adsorption and desorption, respectively).

Catalytic Cycloaddition of CO_2 with Epoxides:

Removal of coordinated H_2O molecules by activation resulted in dehydrated samples of 1−2 with the 1D channels decorated with four Lewis acidic Co^{II} ions. The high thermal stability of the dehydrated samples of **1**−**2** and selective CO_2 uptake properties at room temperature for **1** motivated us to investigate their catalytic properties for heterogeneous cycloaddition of CO_2 with epoxides to generate cyclic carbonates

Prior to catalytic reaction, the samples were activated at 373 K under vacuum for 18 h to generate the active catalyst. PXRD analysis of the activated samples of **1−2** (i.e, **1a** and **2a**) confirmed retention of the original framework structure (Figure S1−S2). Controlled experiments carried out at different temperatures and loadings of tetra-n-butylammonium bromide (TBAB) revealed that the optimum conditions required are the reaction temperature of 80 °C for 12 h with 0.5 mol % (based on Co(II).) catalyst loading and a CO_2 pressure of 1 atm. It was observed that both the catalyst and co-catalyst TBAB are essential for the catalytic reaction. A literature survey revealed that TBAB has been commonly employed as a cocatalyst in the catalytic cycloaddition of CO_2.

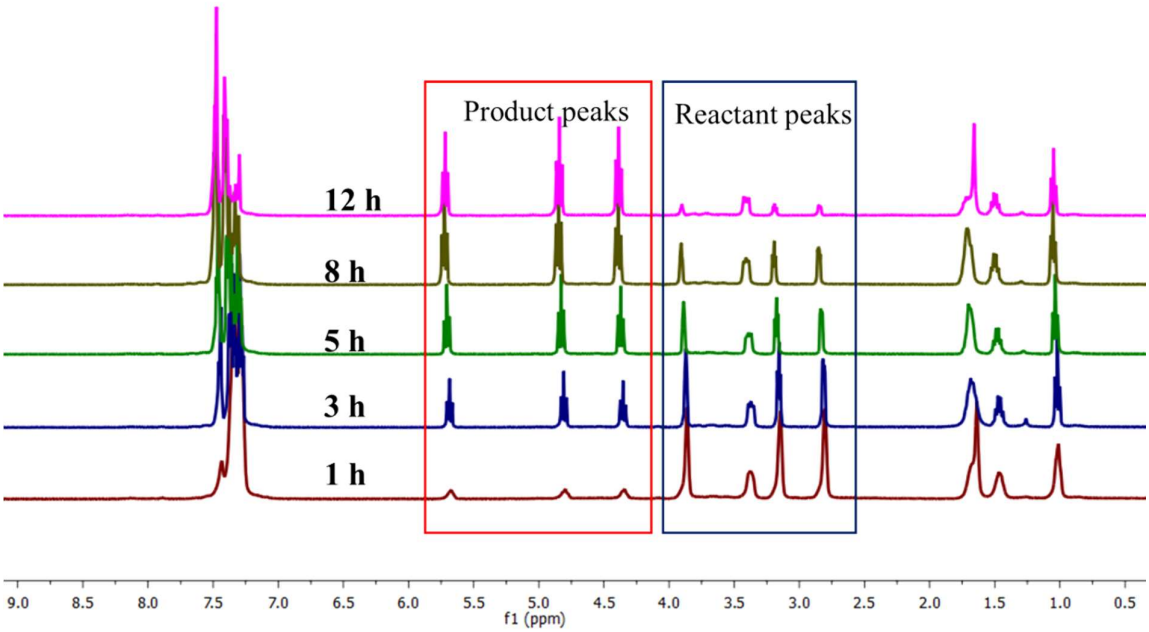

Figure S7: Time-dependent ^1H ($CDCl_3$, 400 MHz) NMR stack plot for the cycloaddition of CO_2 with styrene oxide catalyzed by **1a**, showing gradual increase of peaks at 4.3, 4.8 and 5.6 ppm, due to product, and decrease in the intensity of peaks around 2.7, 3.1 and 3.8 ppm due to styrene oxide.

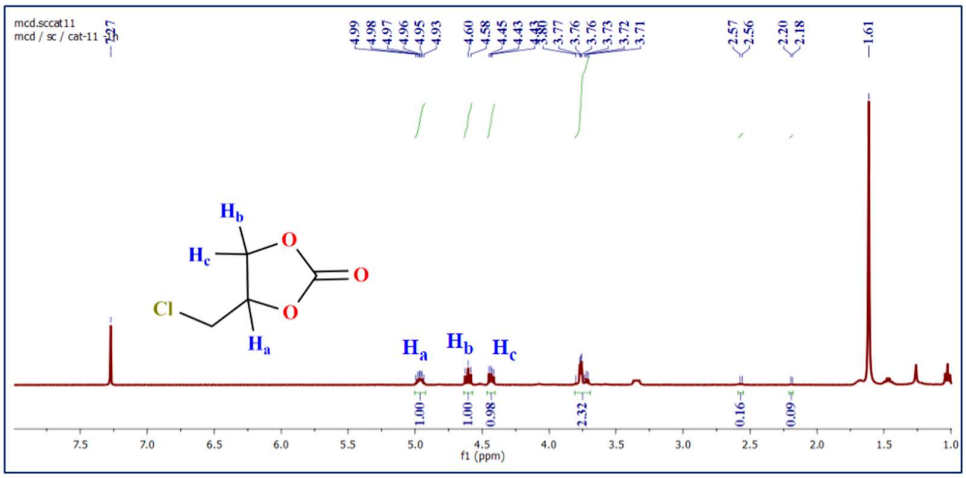

Figure S8: ^{1}H NMR ($CDCl_3$, 400 MHz) spectra for the cycloaddition reaction of CO_2 with 1-chloro-2,3-epoxypropane catalyzed by **1a**.

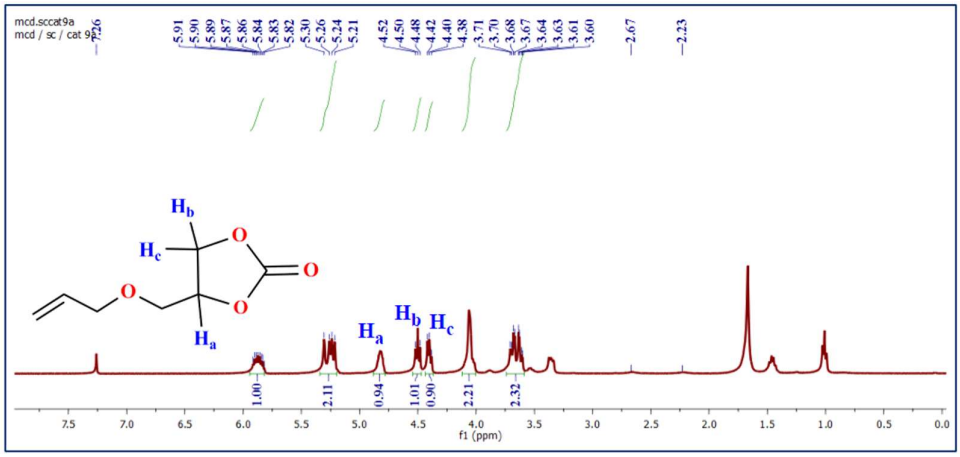

Figure S9: ^{1}H NMR ($CDCl_3$, 400 MHz) spectra for the cycloaddition reaction of CO_2 with 1-allyloxy-2,3-epoxypropane catalyzed by **1a**.

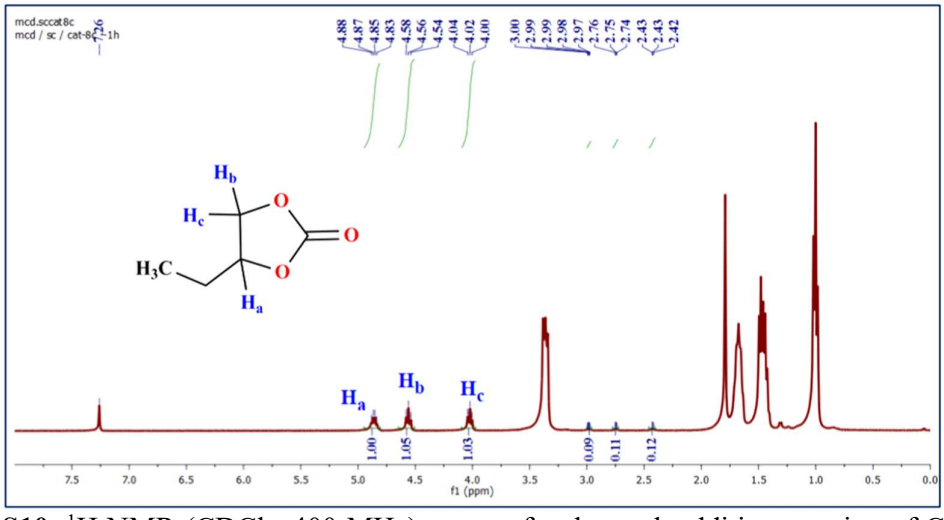

Figure S10: ^{1}H NMR ($CDCl_3$, 400 MHz) spectra for the cycloaddition reaction of CO_2 with 1,2-epoxybutane catalyzed by **1a**.

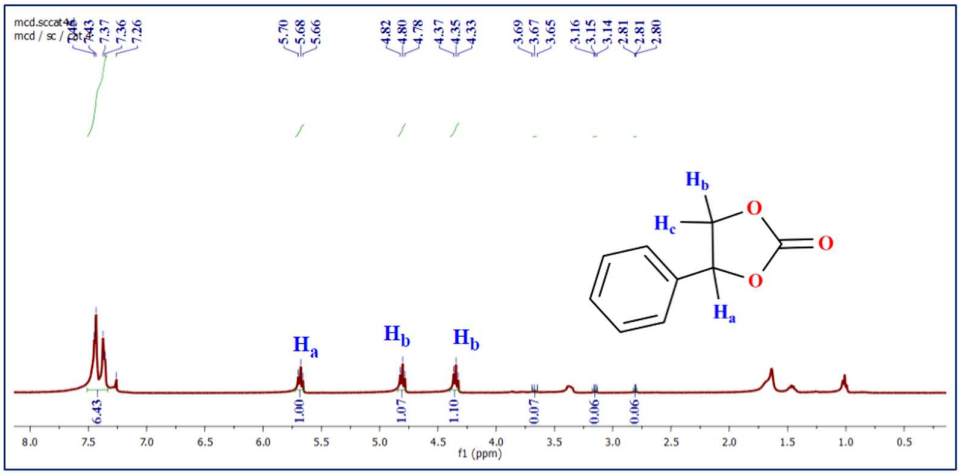

Figure S11: ^{1}H NMR ($CDCl_3$, 400 MHz) spectra for the cycloaddition reaction of CO_2 with 1,2-epoxyethylbenzene catalyzed by **1a**.

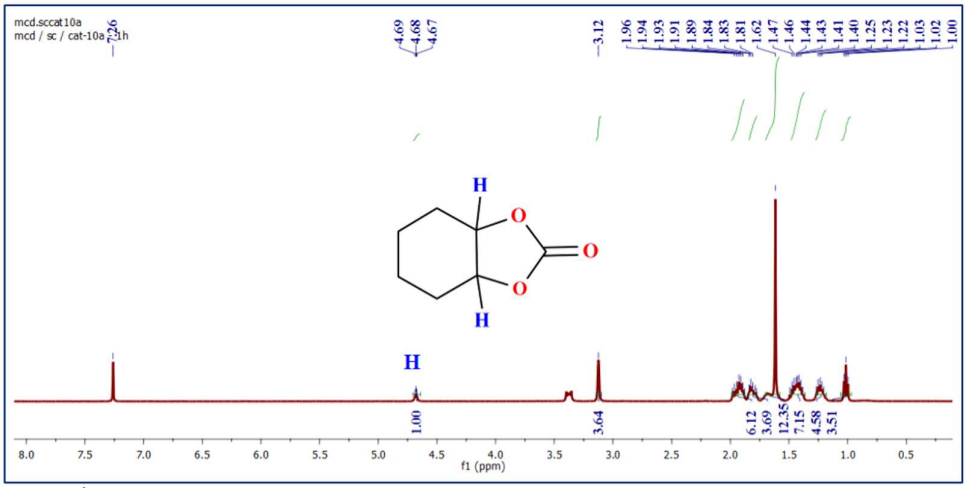

Figure S12: ^{1}H NMR ($CDCl_3$, 400 MHz) spectra for the cycloaddition reaction of CO_2 with 1,2-epoxycyclohexane catalyzed by **1a**.

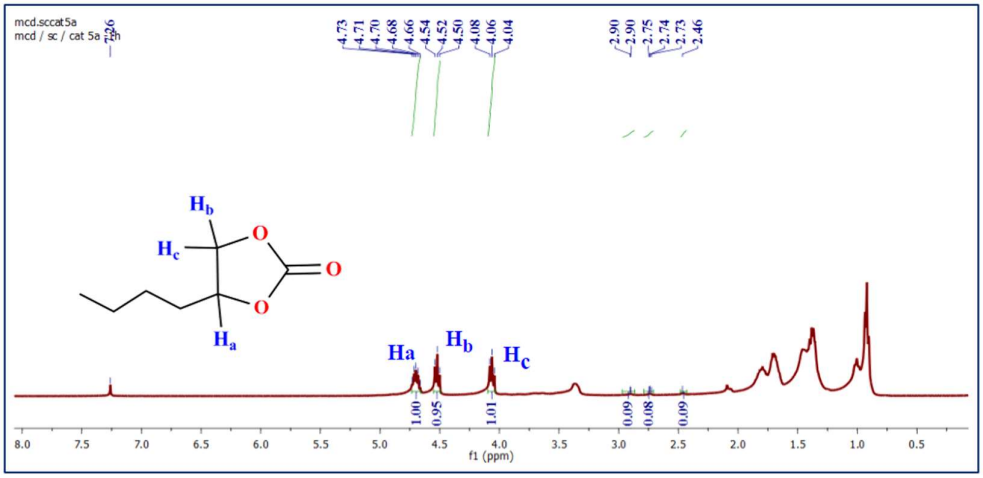

Figure S13: ^{1}H NMR ($CDCl_3$, 400 MHz) spectra for the cycloaddition reaction of CO_2 with 1,2-epoxyhexane catalyzed by **1a**.

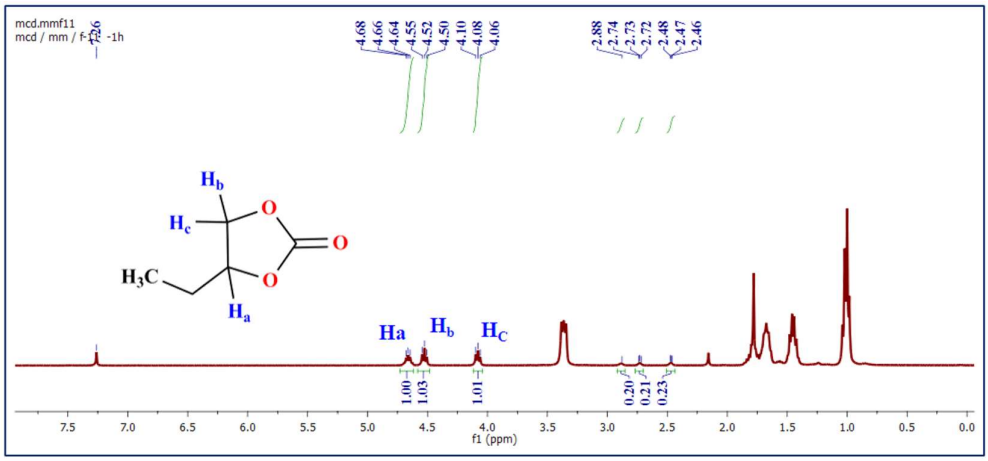

Figure S14: ^{1}H NMR ($CDCl_3$, 400 MHz) spectra for the cycloaddition reaction of CO_2 with 1,2-epoxybutane catalyzed by **2a**.

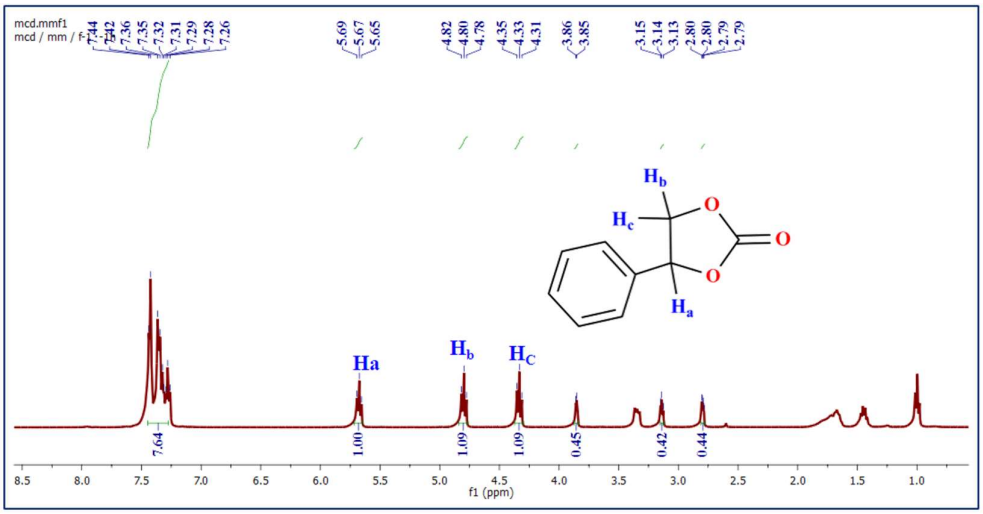

Figure S15: ^{1}H NMR ($CDCl_3$, 400 MHz) spectra for the cycloaddition reaction of CO_2 with 1,2-epoxyethylbenzene catalyzed by **2a**.

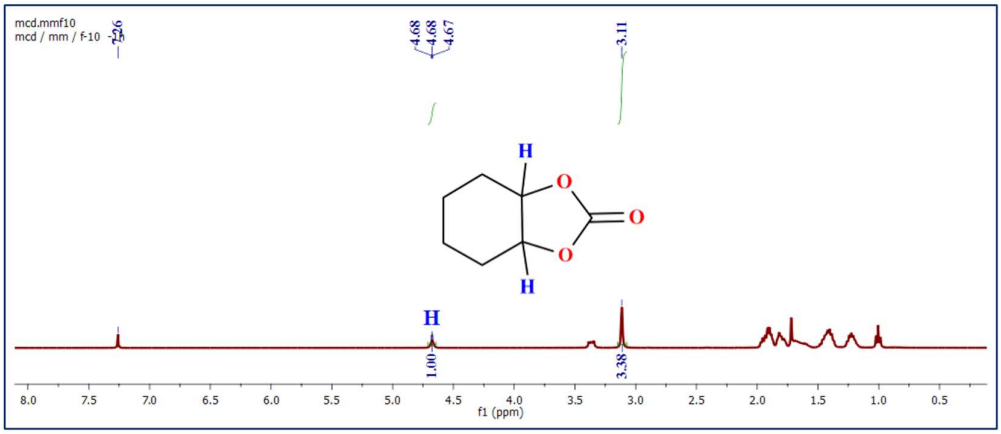

Figure S16: ^{1}H NMR ($CDCl_3$, 400 MHz) spectra for the cycloaddition reaction of CO_2 with 1,2-epoxycyclohexane catalyzed by **2a**.

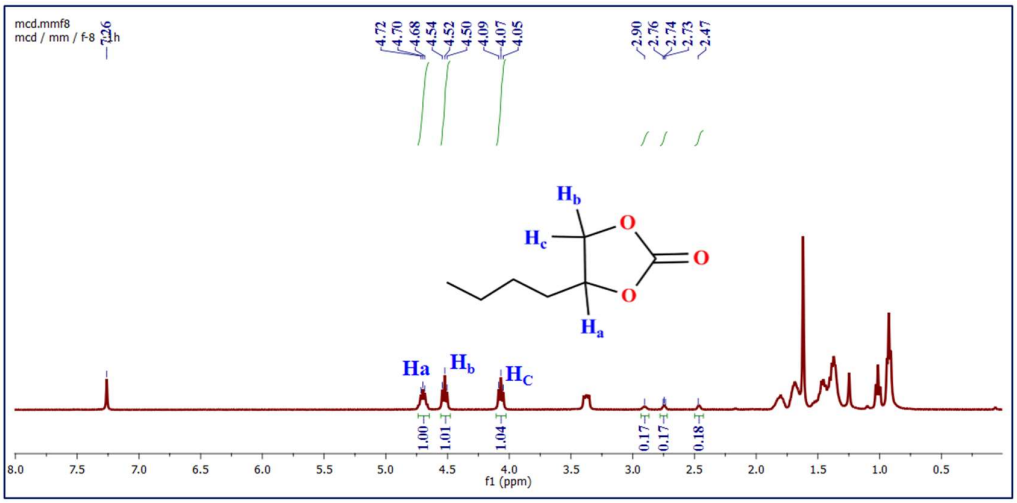

Figure S17: ^{1}H NMR ($CDCl_3$, 400 MHz) spectra for the cycloaddition reaction of CO_2 with 1,2-epoxyhexane catalyzed by **2a**.

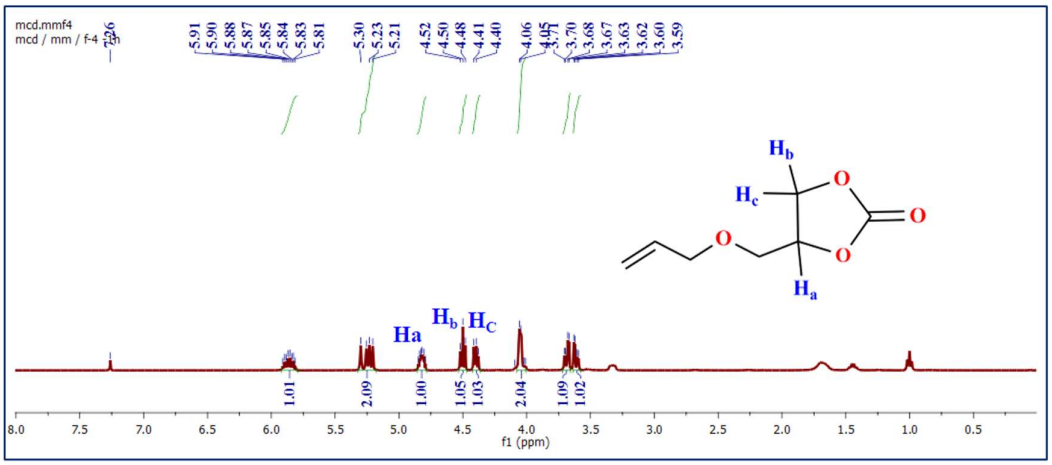

Figure S18: ^{1}H NMR ($CDCl_3$, 400 MHz) spectra for the cycloaddition reaction of CO_2 with 1-allyloxy-2,3-epoxypropane catalyzed by **2a**.

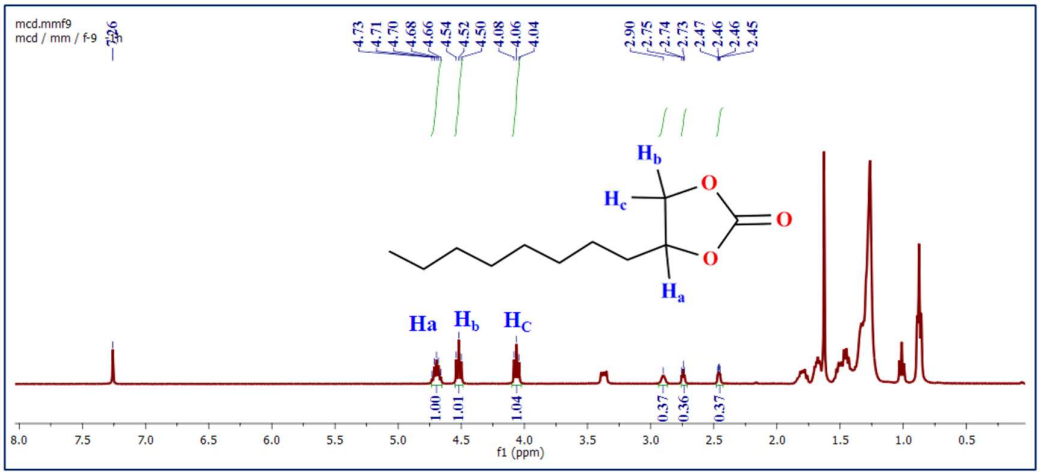

Figure S19: ^{1}H NMR ($CDCl_3$, 400 MHz) spectra for the cycloaddition reaction of CO_2 with 1,2-epoxydecane catalyzed by **2a**.

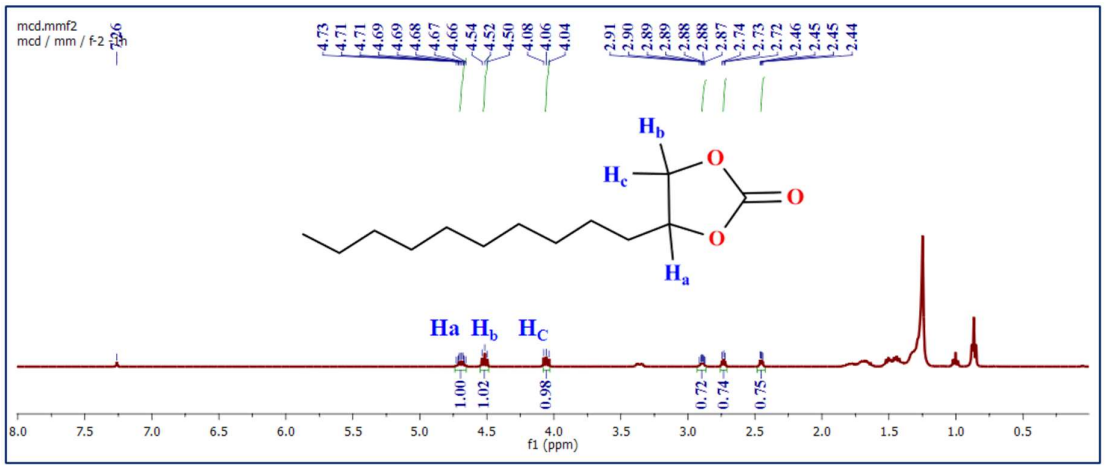

Figure S20: ^{1}H NMR ($CDCl_3$, 400 MHz) spectra for the cycloaddition reaction of CO_2 with 1,2-epoxydodecane catalyzed by **2a**.

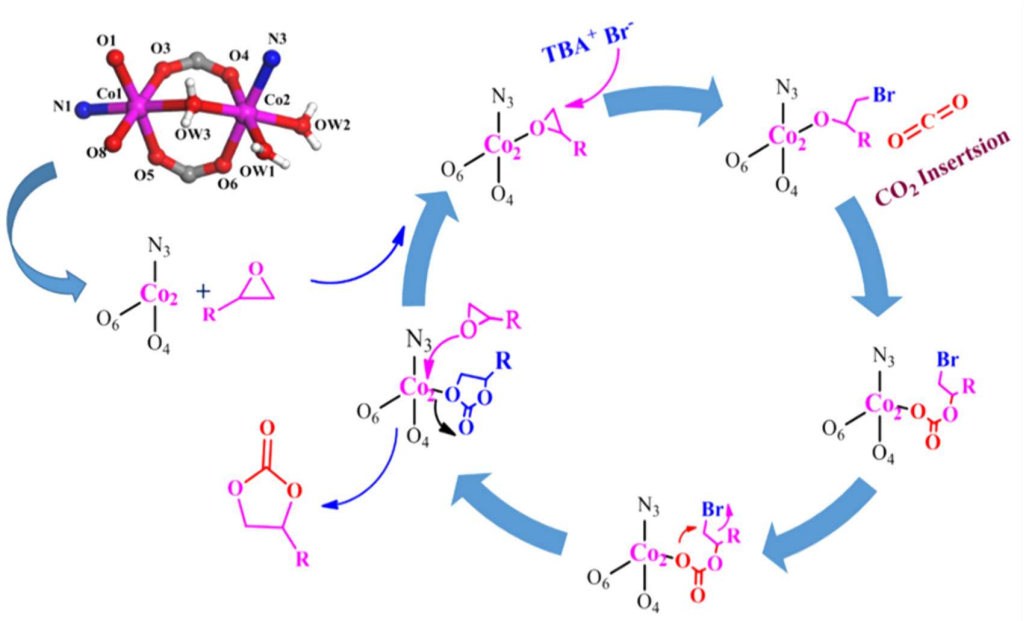

Scheme S1: A tentative reaction mechanism proposed for the cycloaddition of carbon dioxide and epoxides by **1a**.[5,6]

The coupling reaction is initiated by coordination of the epoxide to the Lewis acidic Co(II) center in the frameworks of **1a** and **2a** through the O atom of epoxide leading to activation of the epoxy ring. Consequently, nucleophile Br- anion coming from co-catalyst attacks the less-hindered C atom of the coordinated epoxide in order to open the epoxy ring. This is followed by the interaction of O anion of the opened epoxy ring with CO_2 ring form an alkylcarbonate anion. Further, this intermediate undergoes an intramolecular ring closing step affording the corresponding cyclic carbonate.

Table S6: Comparison of the Catalytic Activity of Various MOFs for the Cycloaddition Reaction of CO_2 with Epoxides.

Catalyst	Epoxide	Time(h)	Pressure (MPa)	Temperature (°C)	Conversion (%)	Ref
IRMOF-1	AGE	6	1.2	120	34	*J. Nanosci. Nanotechnol.* **2013**, *13,* 2307.
IRMOF-3	AGE	6	1.2	120	80	*J. Nanosci. Nanotechnol.* **2013**, *13*, 2307.
$Cu_3(BTC)_2$	EPCH	4	0.7	100	33	*Catal. Today* **2012**, *198*, 215.
ZIF-8	SO	5	0.74	100	55	*Catal. Surv. Asia* **2015**, *19*, 223.
Mg-MOF-74	SO	4	2	100	95	*Nat. Chem.* **2014**, *6*, 673.
UIO-66	SO	4	2	100	94	*Appl. Catal. A* **2013**, *453*, 175.
PCN-224	PO	4	2	100	42	*J. Am. Chem. Soc.* **2013**, *135*, 17105.
MOF-5	PO	4	6	50	97.6	*Nat. Chem.* **2014**, *6*, 673.
ZIF-68	SO	12	1	100	93.3	*Inorg. Chem.* **2016**, *55*, 7291.
1	**SO**	**12**	**1 atm**	**80**	**93**	**This Work**
2	**SO**	**12**	**1atm**	**80**	**86**	**This Work**

EPCH = epichlorohydrin, AGE = allgylglycidyl ether, SO = styrene oxide, and PO = propylene oxide

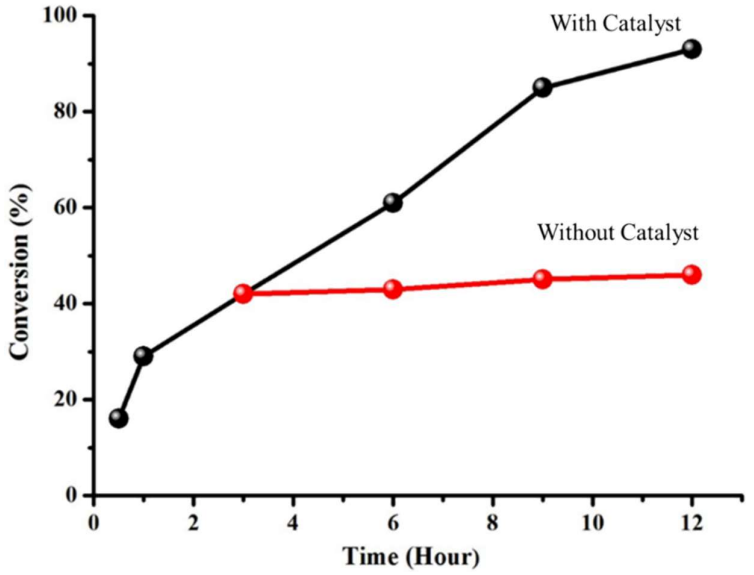

Figure S21: Hot filtration test for the reaction between styrene oxide and CO_2 was performed in the presence of **1a**. After 3 hours of reaction, the catalyst was removed by filtration at the reaction temperature. The product formation in the filtrate under the same reaction conditions was monitored (red line).

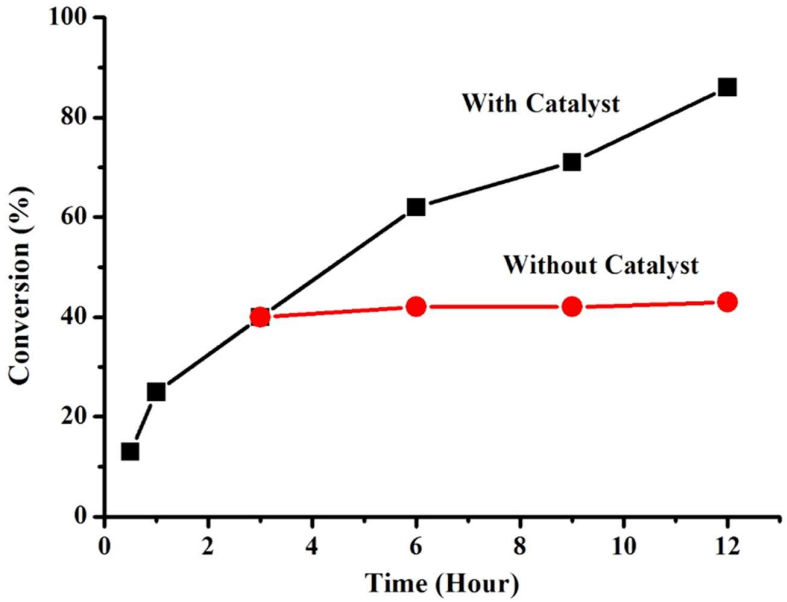

Figure S22: Hot filtration test for the reaction between styrene oxide and CO_2 was performed in the presence of **2a**. After 3 hours of reaction, the catalyst was removed by filtration at the reaction temperature. The product formation in the filtrate under the same reaction conditions was monitored (red line).

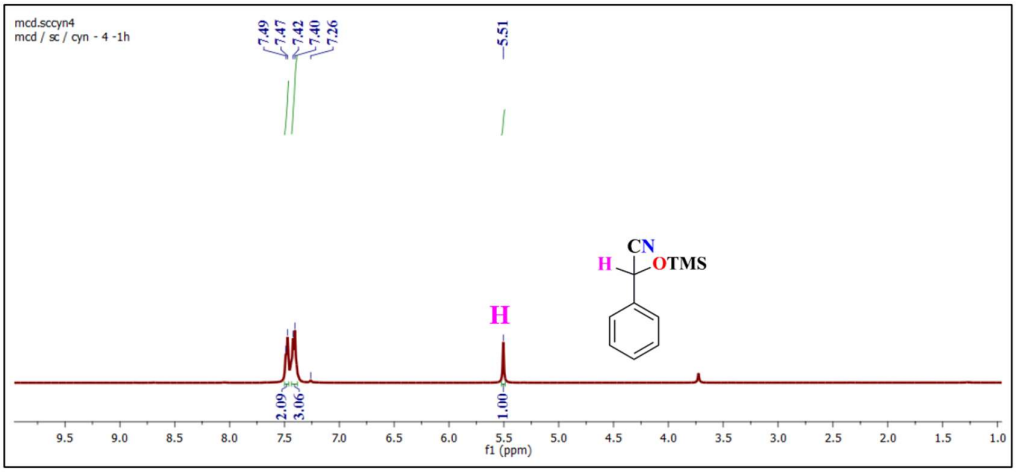

Figure S23: ^{1}H NMR ($CDCl_3$, 400 MHz) spectra for the cyanosilylation reaction of benzaldehyde with trimethylsilyl cyanide catalyzed by **1a**.

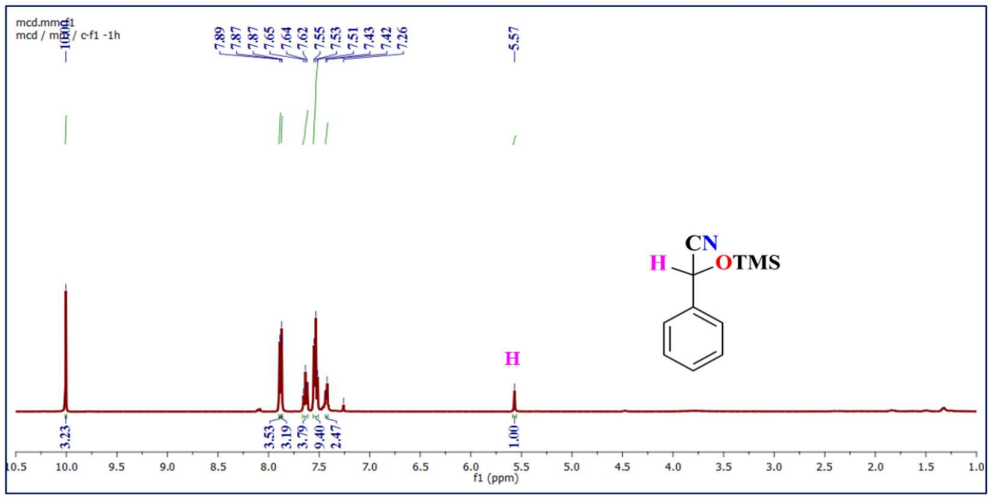

Figure S24: ^{1}H NMR ($CDCl_3$, 400 MHz) spectra for the cyanosilylation reaction of benzaldehyde with trimethylsilyl cyanide catalyzed by **2a**.

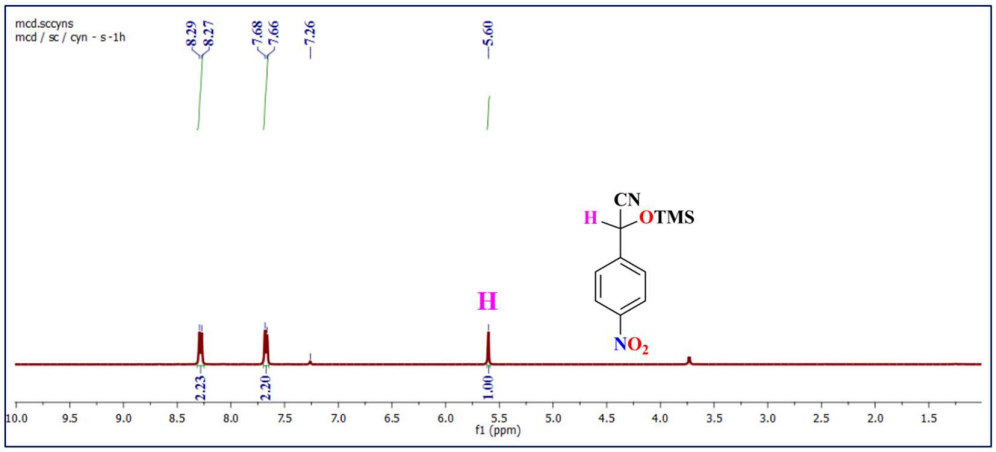

Figure S25: ^{1}H NMR ($CDCl_3$, 400 MHz) spectra for the cyanosilylation reaction of 4-nitrobenzaldehyde with trimethylsilyl cyanide catalyzed by **1a**.

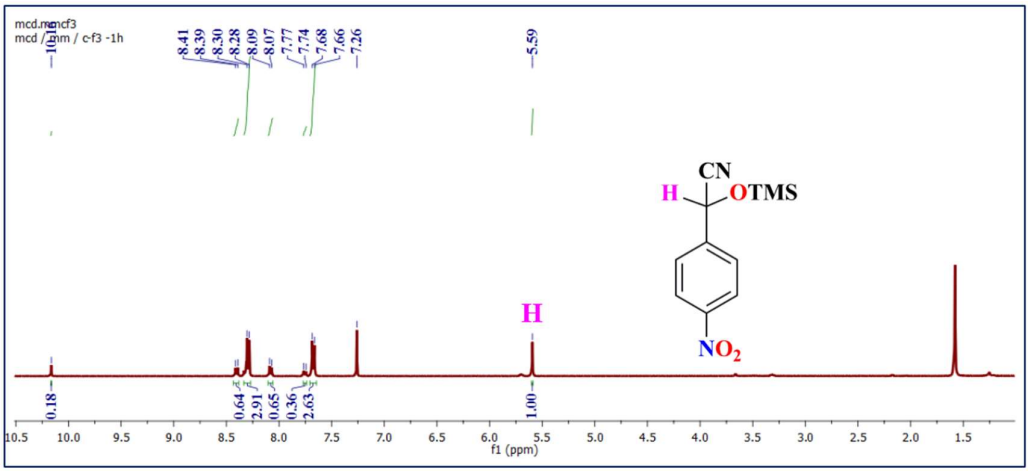

Figure S26: ^{1}H NMR ($CDCl_3$, 400 MHz) spectra for the cyanosilylation reaction of 4-nitrobenzaldehyde with trimethylsilyl cyanide catalyzed by **2a**.

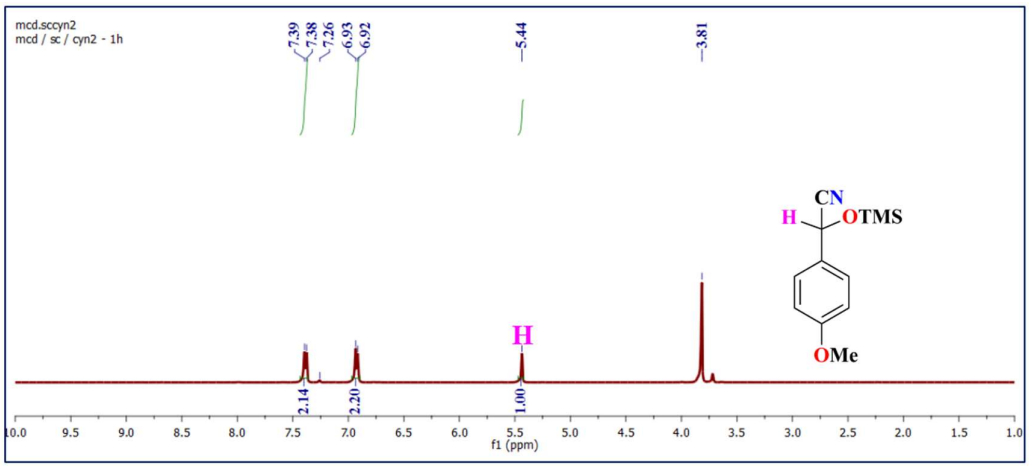

Figure S27: ^{1}H NMR ($CDCl_3$, 400 MHz) spectra for the cyanosilylation reaction of 4-Methoxybenzaldehyde with trimethylsilyl cyanide catalyzed by **1a**.

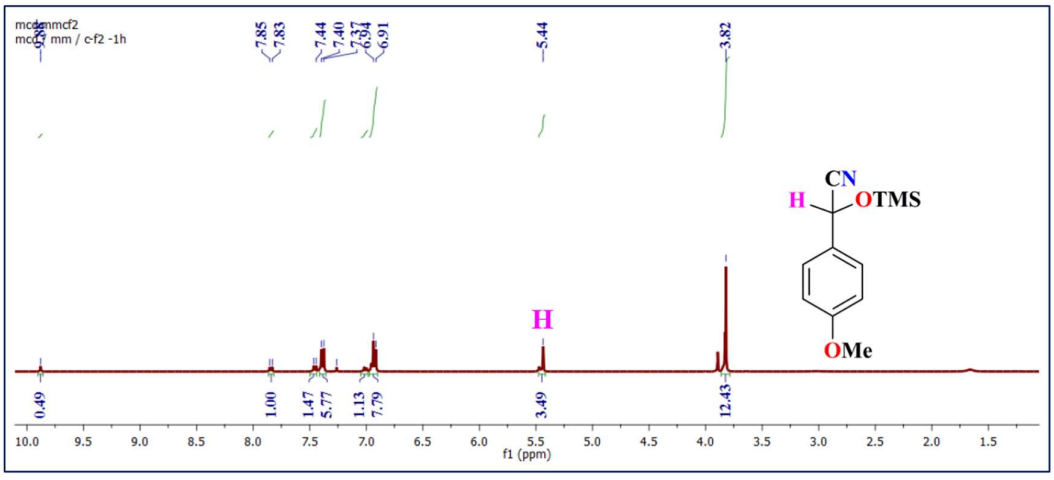

Figure S28: ^{1}H NMR ($CDCl_3$, 400 MHz) spectra for the cyanosilylation reaction of 4-methoxybenzaldehyde with trimethylsilyl cyanide catalyzed by **2a**.

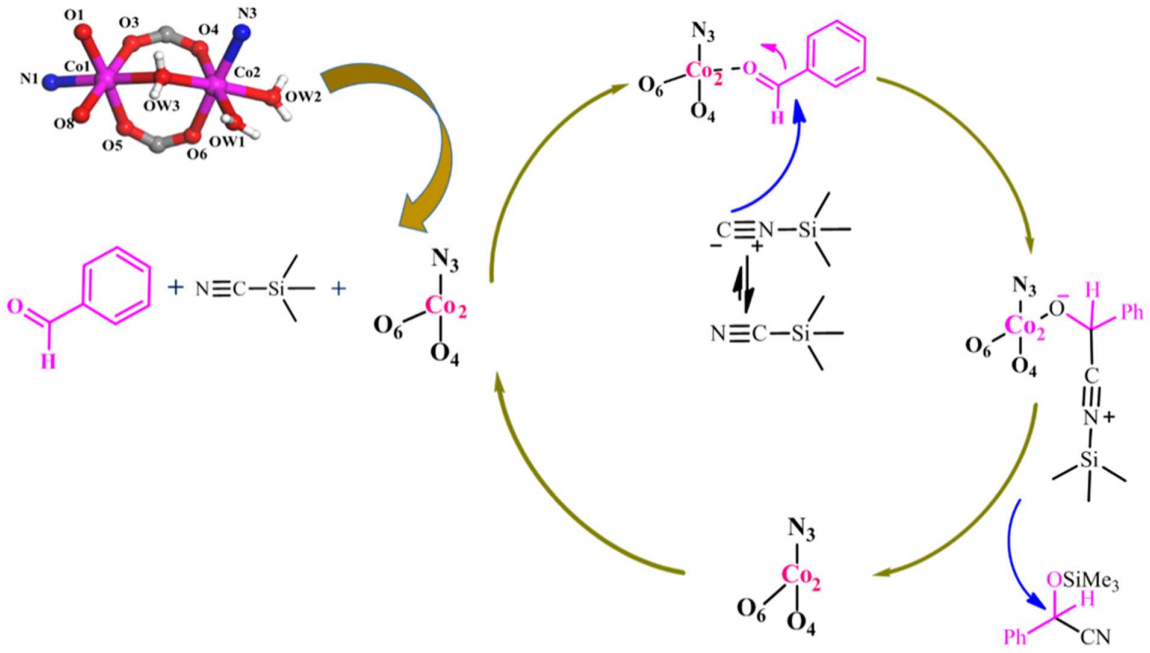

Scheme S2: Proposed mechanism for the cyanosilylation reaction of carbonyl compounds catalyzed by **1a**. Kindly see the references for detailed information. [7]

Table S7: Comparison of the activity of MOFs with those of the catalysts reported for Cyanosilylation reaction with Me_3SiCN and benzaldehyde.

Catalyst	***T*** **(°C)**	**Time**	**Conv. (%)**	**Ref.**
Cu-CP-3	55	4 h	99.8	*J. Mol. Catal. A-Chem.* **2017,** *428*, 17.
CPO-27-Mg	40	2.5 h	19.96	*J. Mol. Catal. A-Chem*. **2014,** *394*, 57.
CPO-27-$Mn_{0.57}Co_{0.43}$	40	1 h	65	*J. Mol. Catal. A-Chem*. **2014,** *394*, 57.
$Cd_2(L)(DMF)_2(H2O)_2$	40	1.5h	97.44	*RSC Adv*. 2015, *5*, 10119.
Sc-MOF	60	12h	90	*Chem. Commun*. **2009,** *45,* 2393.
In-PF-15	50	1.5 h	80	*RSC Adv*. **2015**, *5*, 7058.
UIO-66-H	40	46 h	97	*RSC Adv*. **2015**, *5*, 79216.
M-DUT-4	40	12 h	80	*Chem. Commun.* **2011**, *47*, 3075.
$In_2(DPA)_3(1,10\ Phen)_2.H_2O$	50	20 min	98	*CrystEngComm* **2013**, *15,* 9562.
1	**60**	**6 h**	**96**	**This Work**
2	**60**	**6 h**	**81**	**This Work**

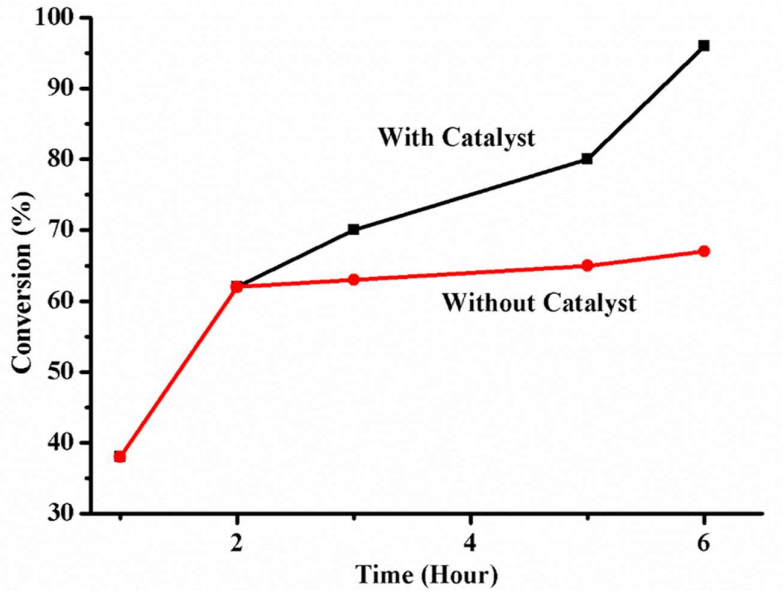

Figure S29: Hot filtration test for the reaction between benzaldehyde and Me_3SiCN was performed in the presence of **1a**. After 2 hours of reaction, the catalyst was removed by filtration. The product formation in the filtrate under the same reaction conditions was monitored (red line).

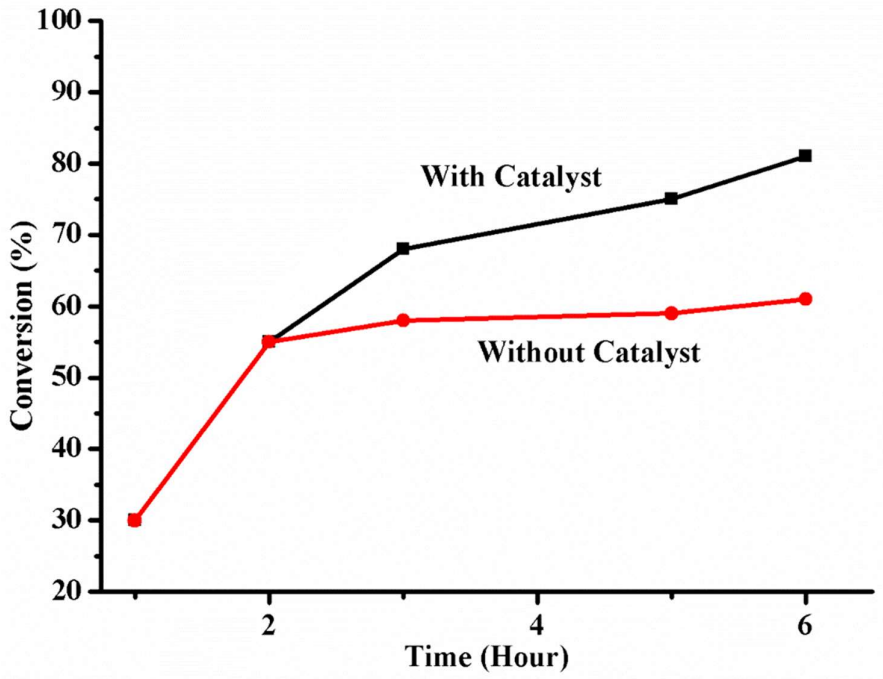

Figure S30: Hot filtration test for the reaction between benzaldehyde and Me_3SiCN was performed in the presence of **2a**. After 2 hours of reaction, the catalyst was removed by filtration. The product formation in the filtrate under the same reaction conditions was monitored (red line).

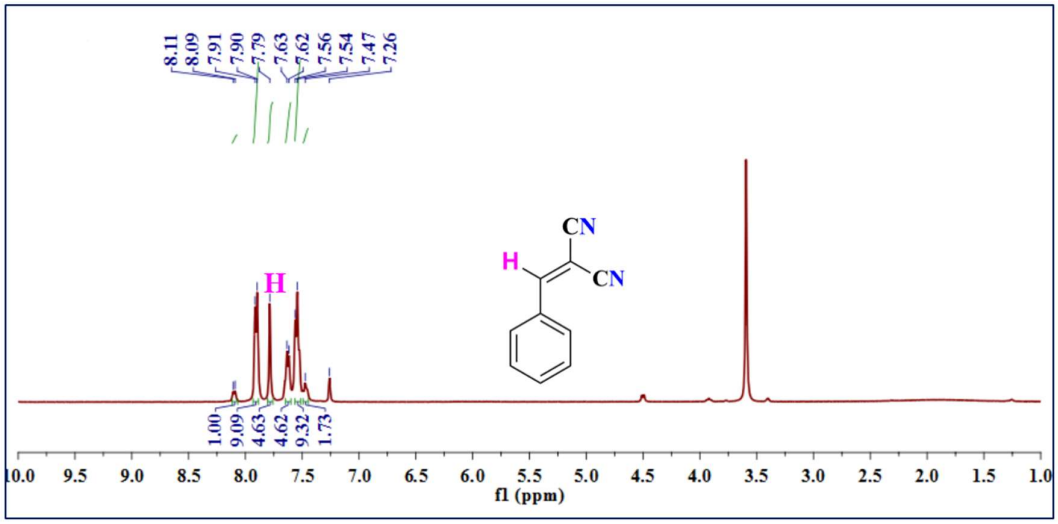

Figure S31: ^{1}H NMR ($CDCl_3$, 400 MHz) spectra for the Knoevenagel reaction of benzaldehyde with malononitrile catalyzed by **1a**.

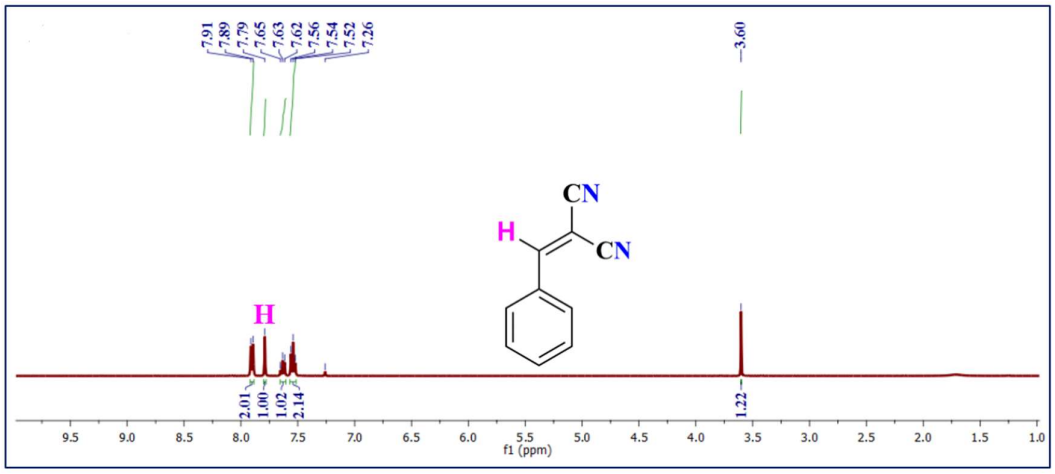

Figure S32: ^{1}H NMR ($CDCl_3$, 400 MHz) spectra for the Knoevenagel reaction of benzaldehyde with malononitrile catalyzed by compound **2a**.

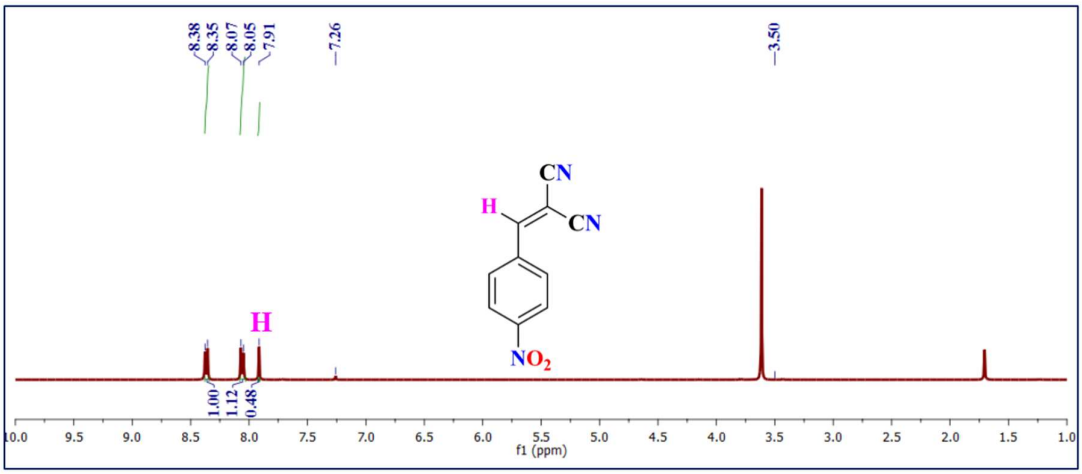

Figure S33: ^{1}H NMR ($CDCl_3$, 400 MHz) spectra for the Knoevenagel reaction of 4-nitrobenzaldehyde with malononitrile catalyzed by **1a**.

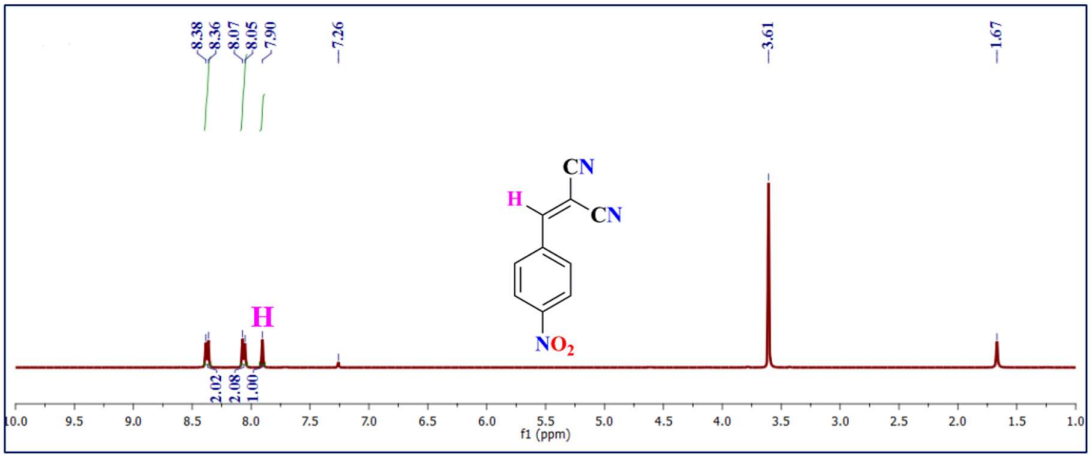

Figure S34: ^{1}H NMR ($CDCl_3$, 400 MHz) spectra for the Knoevenagel reaction of 4-nitrobenzaldehyde with malononitrile catalyzed by **2a**.

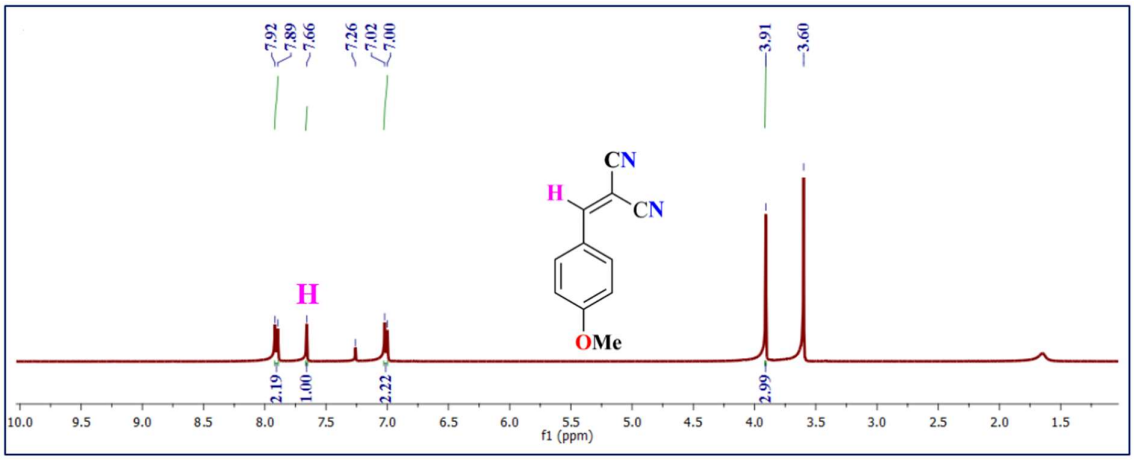

Figure S35: ^{1}H NMR ($CDCl_3$, 400 MHz) spectra for the Knoevenagel reaction of **4**-methoxybenzaldehyde with malononitrile catalyzed by **1a**.

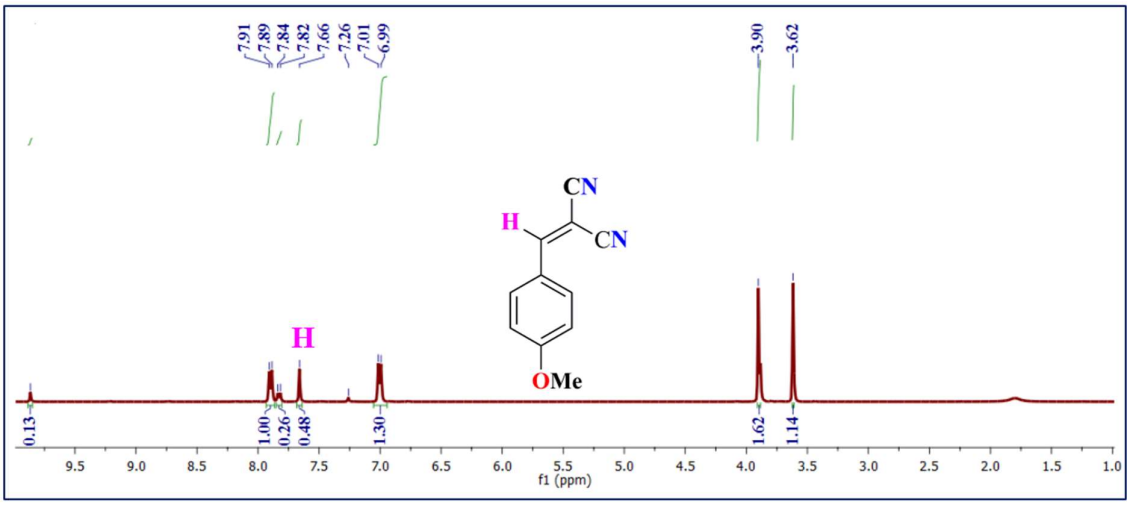

Figure S36: ^{1}H NMR ($CDCl_3$, 400 MHz) spectra for the Knoevenagel reaction of **4**-Methoxybenzaldehyde with malononitrile catalyzed by **2a**.

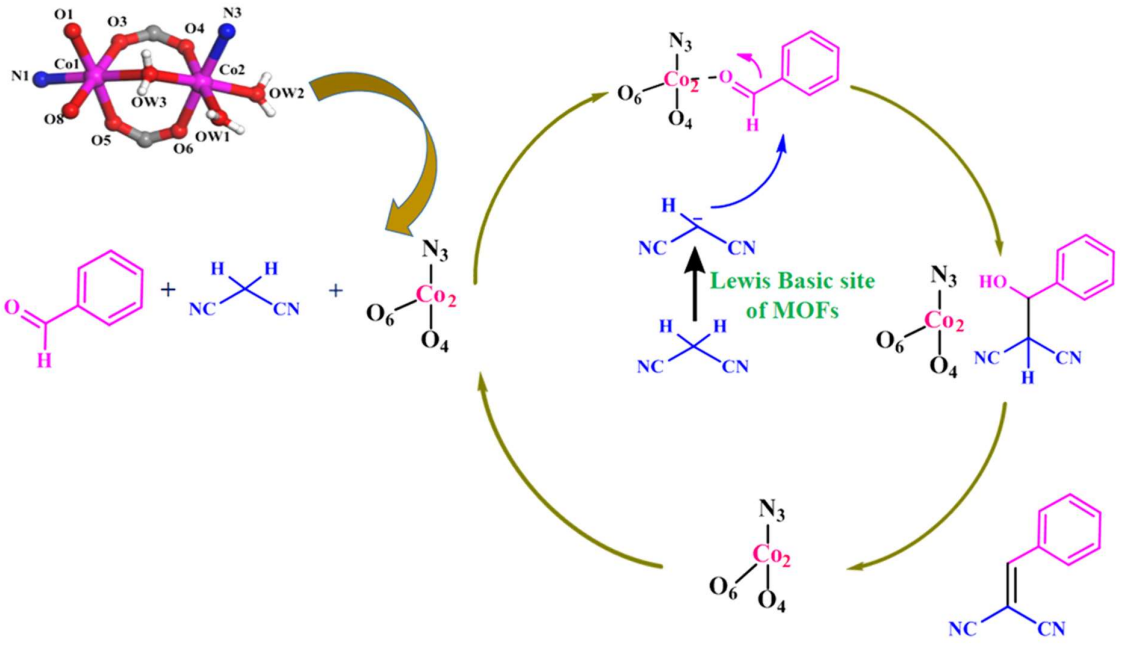

Scheme S3: Proposed mechanism for the Knoevenagel condensation reaction of aldehyde compounds catalyzed by **1a**. Kindly see the references for detailed information: [8,9]

Table S8: Comparison of the activity of MOFs with those of the catalysts reported for Knoevenagel condensation reaction with malononitrile and benzaldehyde.

Catalyst	*T* (°C)	Time	Conv. (%)	Ref.
$[Cd(4btapa)_2(NO_3)_2]\cdot 6H_2O\cdot 2DMF$	RT	12 h	98	*J. Am. Chem. Soc.* **2007**, *129*, 2607.
$[Gd_2(tnbd)_3(DMF)_4]\cdot 4DMF\cdot 3H_2O$	RT	20 min	96	*Chem. – Eur. J.* **2012,** *18*, 6866.
ZIF-8	RT	1 h	97	*Catal. Sci. Technol.* **2011**, *1*, 120.
ZIF-9	RT	2 h	99	*Catal. Sci. Technol.* **2012**, *2*, 521.
$Cu_3(BTC)_2$	60	6 h	88	*Catal. Sci. Technol.* ***2013****, 3, 500.*
DETA-Cr-MIL-101	RT	1 h	97	*CrystEngComm* **2012**, *14*, 4142.
Fe-MIL-101-NH_2, Al-MIL-101-NH_2	80	3 h	90	*MicroporousMesoporous Mater*. **2012**, *164*, 38.
$Zn_2(tpt)_2(p\text{-}BDC\text{-}NH_2)I_2$	60	2 h	99	*Inorg. Chem. Commun.* **2011**, *14*, 1966.
Zn-MOF-NH_2	80	4.5 h	98	*Synlett*. **2016**, *27*, 1433.
CAU-1-NH_2	40	1 h	94	*CrystEngComm* **2017**, *19,* 4187.
1	**60**	**6 h**	**95**	**This work**
2	**60**	**6 h**	**93**	**This work**

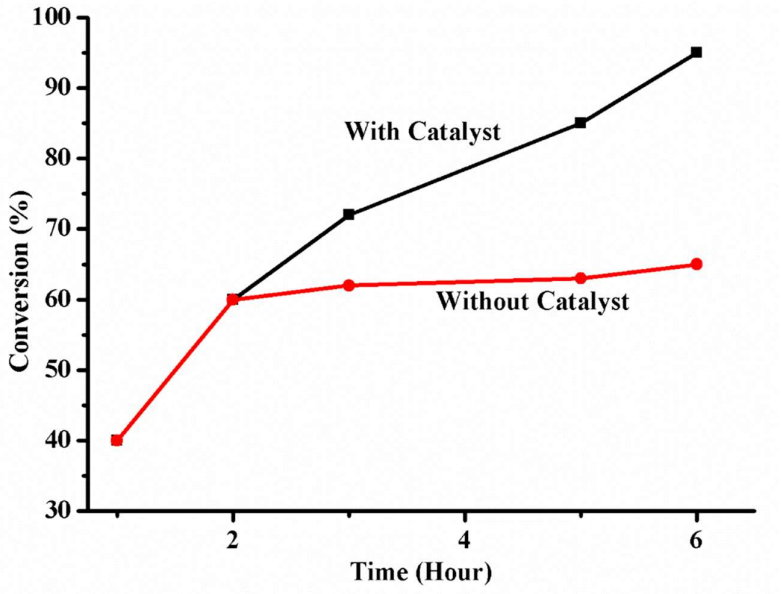

Figure S37: Hot filtration test for the reaction between benzaldehyde with malononitrile was performed in the presence of **1a**. After 2 hours of reaction, the catalyst was removed by filtration. The product formation in the filtrate under the same reaction conditions was monitored (red line).

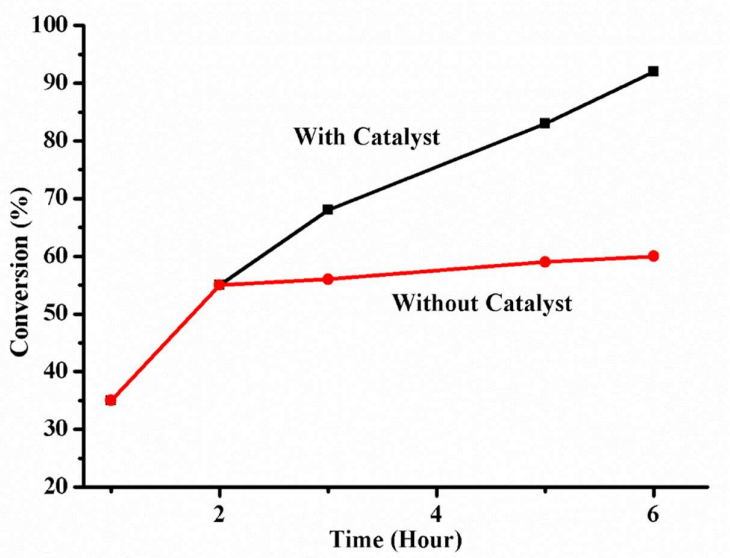

Figure S38: Hot filtration test for the reaction between benzaldehyde with malononitrile was performed in the presence of **2a**. After 2 hours of reaction, the catalyst was removed by filtration. The product formation in the filtrate under the same reaction conditions was monitored (red line).

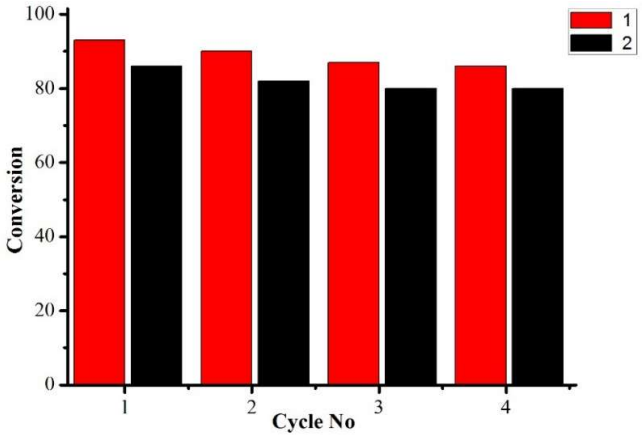

Figure S39: Recyclability test of **1a** (red bar) and **2a** (black bar) up to a minimum four cycles for CO_2 cycloaddition reactions.

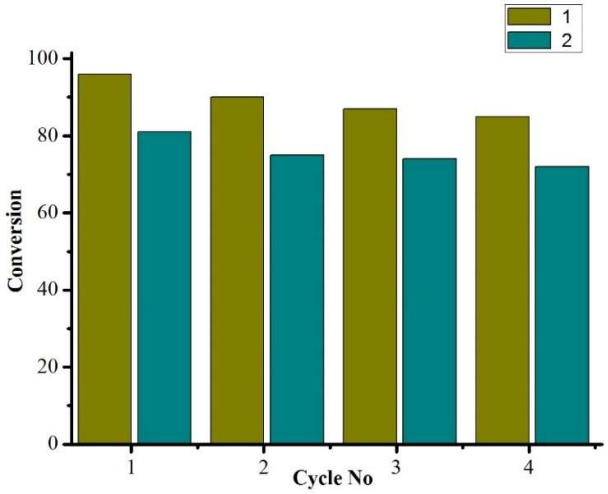

Figure S40: Recyclability test of **1a** (dark yellow bar) and **2a** (dark cyan bar) up to a minimum four cycles for cyanosilylation reactions.

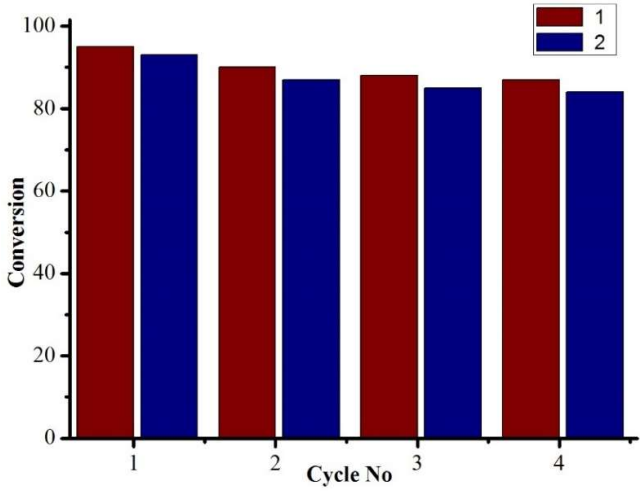

Figure S41: Recyclability test of **1a** (wine bar) and **2a** (blue bar) up to a minimum four cycles for Knoevenagel condensation reaction.

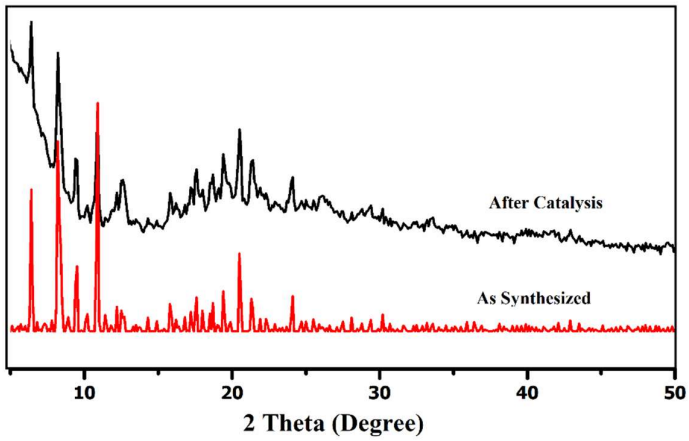

Figure S42: The PXRD pattern of **1a** as synthesized (red) and after catalysis (black).

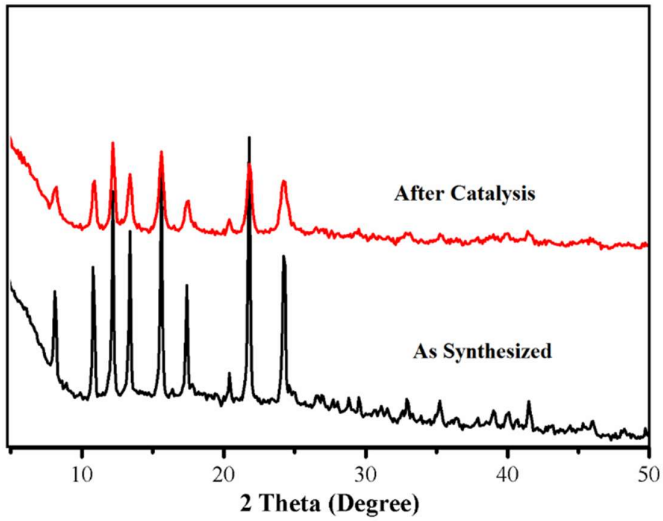

Figure S43: The PXRD pattern of **2a** as synthesized (black) and after catalysis (red).

‖ S.C. and S.C.P. contributed equally to this work.

REFERENCES:

[1] SAINT+, 6.02ed, Bruker AXS, Madison, WI, **1999**.

[2] XPREP, 5.1 ed. Siemens Industrial Automation Inc., Madison, WI, **1995**.

[3] Sheldrick, G. M. *SHELXTL ™Reference Manual*: version 5.1, Bruker AXS, Madison, WI, **1997**.

[4] Sheldrick, G. M. Crystal Structure Refinement with SHELXL. *Acta Cryst C*, **2015**, *71*, 3.

[5] North, M.; Pasquale, R. Mechanism of Cyclic Carbonate Synthesis from Epoxides and CO_2. *Angew. Chem., Int. Ed*. **2009**, *48*, 2946−2948.

[6] He, H.; Perman, J. A.; Zhu, G.; Ma, S. Metal-Organic Frameworks for CO_2 Chemical Transformations. *Small* **2016**, *12*, 6309-6324.

[7] Zhang, Z.; Chen, J.; Bao, Z.; Chang, G.; Xing, H.; Ren, Q. Insight into the Catalytic Properties and Applications of Metal Organic Frameworks in the Cyanosilylation of Aldehydes. *RSC Adv.* **2015**, *5*, 79355-79360.

[8] Hasegawa, S.; Horike, S.; Matsuda, R.; Furukawa, S.; Mochizuki, K.; Kinoshita, Y.; Kitagawa, S. Three-Dimensional Porous Coordination Polymer Functionalized with Amide Groups Based on Tridentate Ligand: Selective Sorption and Catalysis. *J. Am. Chem. Soc*. **2007**, *129*, 2607-2614.

[9] Yao, C.; Zhou, S.; Kang, X.; Zhao, Y.; Yan, R.; Zhang, Y.; Wen, L. A Cationic Zinc–Organic Framework with Lewis Acidic and Basic Bifunctional Sites as an Efficient Solvent-Free Catalyst: CO_2 Fixation and Knoevenagel Condensation Reaction. *Inorg. Chem.* **2018**, *57*, 11157−11164.